



## Letter

# Role of multi-phonon and high-spin states on the quasi-elastic barrier distributions of massive systems

P.W. Wen<sup>a, ID</sup>, O. Chuluunbaatar<sup>b,c,d, ID,\*</sup>, P. Descouvemont<sup>e, ID,\*</sup>, A.A. Gusev<sup>b,d,f, ID</sup>,  
C.J. Lin<sup>a,g, ID,\*</sup>, S.I. Vinitisky<sup>b,h, ID</sup>

<sup>a</sup> China Institute of Atomic Energy, 102413 Beijing, China

<sup>b</sup> Joint Institute for Nuclear Research, Dubna, 141980 Moscow region, Russia

<sup>c</sup> Institute of Mathematics and Digital Technology, Mongolian Academy of Sciences, 13330 Ulaanbaatar, Mongolia

<sup>d</sup> School of Applied Sciences, Mongolian University of Science and Technology, Ulaanbaatar 14191, Mongolia

<sup>e</sup> Département de Physique, CP229, Université Libre de Bruxelles (ULB), B1050 Brussels, Belgium

<sup>f</sup> Dubna State University, 141980 Dubna, Russia

<sup>g</sup> College of Physics and Technology & Guangxi Key Laboratory of Nuclear Physics and Technology, Guangxi Normal University, 541004 Guilin, China

<sup>h</sup> Peoples' Friendship University of Russia (RUDN University), 117198, 6 Miklukho-Maklaya St, Moscow, Russia



## ARTICLE INFO

Editor: B. Blank

**Keywords:**

Quasi-elastic reaction  
Barrier distribution  
Coupled-channel equation  
Rotational coupling

## ABSTRACT

Back-angle quasi-elastic (QE) scattering provides critical barrier information in massive nuclear reactions leading to the synthesis of superheavy nuclei. The shapes and peaks of QE barrier distributions serve as fingerprints of nuclear structures and reaction dynamics. Couplings to collective movements can lead to distinctive peaks in the barrier distributions, but the role of multi-phonon and high-spin states has not been thoroughly investigated. In this work, we extend the high-accuracy R-matrix method and the finite element method to solve coupled-channel equations for massive systems. These two methods are demonstrated to be more stable than the widely used modified Numerov method and allows us to include more vibrational and rotational couplings. Using the reactions  $^{48}\text{Ti} + ^{208}\text{Pb}$  and  $^{51}\text{V} + ^{248}\text{Cm}$  as examples, calculations show that multi-phonon and high-spin states significantly smooth the barrier distributions, improving the agreement with experimental data. The comparison between the coupled-channel results and those obtained from the orientation average formula is examined. This work can advance the study of superheavy element synthesis by providing reliable barrier information and capture cross sections based on constraints from QE reactions.

Quasi-elastic (QE) scattering, which includes elastic, inelastic, and few-nucleon transfer processes, serves as a good counterpart to fusion reactions and is a crucial method for studying the mutual influence between complex nuclear structure and reaction dynamics [1–6]. The barrier distributions of fusion and QE reactions provide fingerprints of the couplings between the relative motion of two nuclei and the motion of nucleons within each nucleus [7]. Different shapes of QE barrier distributions exhibit specific features of couplings to structures or reaction channels in the coupled-channel (CC) approach. For instance, a second peak of the barrier distribution at higher energy occurs due to the coupling to target phonon states for  $^{16}\text{O} + ^{144}\text{Sm}$  [8]. Conversely, the quadrupole  $\beta_2$  and hexadecapole  $\beta_4$  deformation parameters can be pre-

cisely determined based on the QE barrier distributions for nuclei such as  $^{152}\text{Sm}$ ,  $^{170}\text{Er}$ , and  $^{174}\text{Yb}$  [9], and also for  $^{24}\text{Mg}$  [10] and  $^{28}\text{Si}$  [11], which are usually difficult to determine by other types of experiments.

Similarly, the pronounced double-peaked barrier distribution for  $^{20}\text{Ne} + ^{90}\text{Zr}$  can be explained by the coupling to the rotational band of the projectile [12]. However, for  $^{20}\text{Ne} + ^{92}\text{Zr}$ , the large number of single-particle energy levels of  $^{92}\text{Zr}$  obscures the structure of  $^{20}\text{Ne}$ . It was demonstrated that, due to the extra presence of two neutrons beyond the magic shell, the  $^{92}\text{Zr}$  nucleus has many weakly coupled, non-collective excited states, and the couplings with these single-particle states cause dissipation in tunneling and smooth the barrier distribution [13]. On the other hand, for heavier systems, single-particle excitations do not

\* Corresponding authors.

E-mail addresses: [chuka@jinr.ru](mailto:chuka@jinr.ru) (O. Chuluunbaatar), [pierre.descouvemont@ulb.be](mailto:pierre.descouvemont@ulb.be) (P. Descouvemont), [cjlin@ciae.ac.cn](mailto:cjlin@ciae.ac.cn) (C.J. Lin).

<https://doi.org/10.1016/j.physletb.2025.139383>

Received 27 November 2024; Received in revised form 5 March 2025; Accepted 7 March 2025

appear to be sufficient, and the multinucleon transfer channel has been indicated to be able to further smooth the barrier distributions [14–17].

Furthermore, the height and shape of the fusion and QE barrier distributions are key quantities for choosing the bombarding energy in fusion reactions leading to the synthesis of superheavy elements. Since the extraction of fusion barrier distributions for the synthesis of superheavy nuclei is extremely difficult, QE experiments have been widely performed to provide this information in major laboratories worldwide. For instance, QE barrier distributions have been measured for a series of light projectiles including  $^{48}\text{Ti}$ ,  $^{54}\text{Cr}$ ,  $^{56}\text{Fe}$ ,  $^{64}\text{Ni}$ ,  $^{70}\text{Zn}$ , and  $^{86}\text{Kr}$  on a  $^{208}\text{Pb}$  target [18,19]. It has been found that the centroids of the barrier distributions show deviations from those predicted by several potential models. A systematic study of these reactions based on the CC approach showed that triple-octupole phonon excitations in the  $^{208}\text{Pb}$  target are important to improve the description of the experimental barrier distributions [20]. However, there is still a significant discrepancy between theoretical and experimental data, especially regarding the overall smoothness of the experimental data compared to the isolated peaks predicted by the CC calculations.

The heaviest element that has been synthesized to date is oganesson with charge number  $Z = 118$  [21]. Synthesizing the element with  $Z = 119$  is a challenging and highly competitive research topic worldwide. In Refs. [22–24], heavier targets in QE reactions such as  $^{238}\text{U}$  and  $^{248}\text{Cm}$  are involved to study the relationship between QE barrier distributions and the optimum incident energy to synthesize superheavy elements up to  $Z = 119$ . In the theoretical calculations, the potential orientation average (OA) of the deformed targets was considered. This method significantly decreases the number of coupled channels by reducing a high-dimensional coupling problem to the average of results with a smaller number of couplings. Meanwhile, numerical instability problems that might be encountered in solving the CC equations with many couplings of the target were not avoided using the modified Numerov (MN) method [2,25,26], as has been shown for massive reactions such as  $^{48}\text{Ti} + ^{232}\text{Th}$  [27]. The experimental data can be described to a certain extent for these massive QE reactions, which allows for establishing an empirical relationship between the side barrier height and the optimal incident energy for the synthesis of superheavy nuclei [23].

As demonstrated in Ref. [28], up to four-phonon excitations are necessary to reproduce the fusion data of  $^{64}\text{Ni} + ^{74}\text{Ge}$ . Including excitations up to five phonons of the soft octupole mode in  $^{96}\text{Zr}$  gives the best description of the barrier distribution for  $^{48}\text{Ca} + ^{96}\text{Zr}$  [29]. However, these multi-phonon vibrational excitations have not been studied for massive reactions like the above-mentioned  $^{48}\text{Ti} + ^{208}\text{Pb}$  [20]. Besides, the actinide nucleus  $^{248}\text{Cm}$  as the target in QE reactions has a well-measured rotational band from  $0^+$  to  $30^+$  [30]. The excitation energy of the first  $2^+$  state is only 43.4 keV, exhibiting a strong deformation effect. However, the direct study of the high rotational excitations by including them in the CC equations has not been performed yet. It would be interesting to investigate the roles played by more vibrational and rotational excitations in the barrier distributions for these massive QE reactions, which forms the main motivation of this work.

For the vibrational and rotational couplings, we follow the same theoretical CC framework as in our previous works [31,32]. For the sake of simplicity, we do not repeat them here. The detailed formulas for calculating various nuclear reactions observables and how to construct the couplings have been well addressed in many previous works [1,2,20,31]. To solve the CC equations, the MN method is widely used to integrate the equations from a minimum distance with a step size  $R_{\text{step}}$  to a large distance  $R_{\text{max}}$ , where the wave function reaches its asymptotic behavior [25,26]. The matching to the Coulomb functions provides the scattering matrix. A larger  $R_{\text{step}}$  will easily cause fluctuations, and we use a very tiny  $R_{\text{step}}$ , namely 0.0001 fm, to reach high accuracy.

As mentioned above, the widely used MN method could have numerical instability problems when there are many couplings in the solving of the CC equation for massive reactions [20,27]. In this work,

we apply two other numerical methods, namely the R-matrix (RM) method [33–36] and the finite element method (FEM) [31,32,37–43], to solve the high-dimensional CC equations of the massive QE reactions. These methods are known for their numerical stability and accuracy, especially when dealing with complex coupling schemes.

In the RM method, the configuration space is divided into two regions: the internal region and the external region. The channel radius  $R_{\text{max}}$  acts as the boundary between these regions. The internal region is further divided into a number of intervals, and Legendre-type polynomials are used as basis functions, which permit simple calculations of the matrix elements. The propagation method is used to efficiently handle large channel radii without requiring a large number of basis functions [35]. Closed channels are treated straightforwardly, avoiding the numerical issues associated with exponentially growing components in finite difference methods. The number of intervals  $N_s$  and the number of basis functions  $N_R$  can be set as  $N_s = 600$  and  $N_R = 6$ , which are sufficiently large to achieve high accuracy in the following massive calculations. For light reactions, a much smaller  $N_s$  would be adequate to achieve stable results.

The FEM provides an improved numerical accuracy over the Numerov method as shown in Refs. [37–39]. In our implementation, we divide the large distance into smaller parts, namely the finite elements, and then systematically recombine all sets of element equations into a global system of equations using the variation method [37–39,42]. In each divided finite element, the Lagrange interpolation polynomial is used as the basis function. We use the sixth order in this study to keep the smoothness of the cross sections and wave functions. The distance from zero to  $R_{\text{max}}$  is divided into NMESH uniform intervals, which are automatically determined based on the incident energy and reactions. The value of NMESH could be up to 1000 for massive reactions. The computational speeds of the FEM and RM methods are comparable when NMESH is near  $N_s$ . The running speed of MN method depends strongly on  $R_{\text{step}}$ . However, to achieve comparable accuracy, both the RM and FEM methods are significantly faster than the MN method for solving CC equations with a large number of coupled channels as observed in our test. Furthermore, as the number of couplings increases, the speed advantage of the RM and FEM methods becomes even more pronounced. In this work, we intentionally use sufficiently high parameters across the three methods, such as large  $R_{\text{max}}$ ,  $N_s$ ,  $N_R$ , NMESH, and a very small  $R_{\text{step}}$ . Instead of optimizing the parameters for different couplings and reactions to save computational time, we aim to test whether stable results can be reliably obtained under these conditions by the three methods.

To describe QE reactions, imaginary potentials are included to represent absorption channels, and normal boundary conditions are applied [2]. The calculations are carried out for different coupling schemes. As a test of the methods, we first consider as benchmark the two-channel problem  $^{16}\text{O} + ^{44}\text{Ca}$  ( $0^+$ ,  $2^+$ ), which has been studied using the RM method [35] and iterative methods in the Numerov algorithm [44,45]. The  $R_{\text{max}}$  value is set as 30 fm for this light reaction. We adopt the same potential parameters as in previous works. The real and imaginary Woods-Saxon potential parameters are  $V_0 = 110$  MeV,  $W_0 = 20$  MeV,  $R_R = R_I = 1.2$  fm,  $a_R = a_I = 0.5$  fm. The excitation energy of the first vibrational state for  $^{44}\text{Ca}$  is 1.156 MeV, and the deformation parameter  $\beta_2 = 0.4$ , consistent with Ref. [35]. The Coulomb barrier height is 23.03 MeV.

The maximum angular momentum  $L_{\text{max}}$  is usually set as a large enough value in previous works [26]. Since  $L_{\text{max}}$  could change from less than  $100 \hbar$  for the light reactions to more than  $1000 \hbar$  for massive reactions in this study, the algorithm is improved to find the value automatically by judging whether the results of both QE and fusion cross sections have come to a stable value. This procedure guarantees the convergence of the calculations and avoids the waste of calculation time. For the light reaction  $^{16}\text{O} + ^{44}\text{Ca}$ ,  $L_{\text{max}}$  varies up to about  $100 \hbar$ . Fig. 1 in the supplementary material (upper panel) shows the variation of the QE cross section relative to the Rutherford cross section with  $L_{\text{max}}$ .

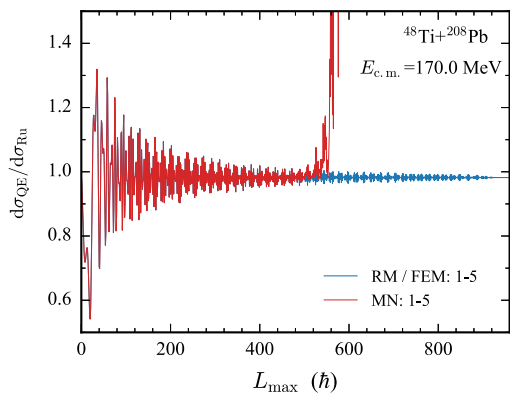


**Fig. 1.** The back-angle QE cross section relative to the Rutherford cross section as a function of  $L_{\max}$  for  $^{48}\text{Ti} + ^{208}\text{Pb}$  at deep sub-barrier energy  $E_{c.m.} = 170.0$  MeV, where the correct value should be close to one. The number combinations in the legend denote the number of phonons used in vibrational couplings for the projectile and the target of this reaction. For example, 1-5 means the phonon numbers  $N_{\text{vib}}^{\text{Proj}} = 1$  and  $N_{\text{vib}}^{\text{Targ}} = 5$ . The Coulomb barrier height is 195.40 MeV.

The calculations are performed at the back-angle  $180^\circ$  and a close barrier energy  $E_{c.m.} = 23$  MeV. All three methods (RM, FEM, MN) produce consistent results at all maximum angular momenta. Fig. 1 in the supplementary material (lower panel) presents the QE cross sections relative to the Rutherford cross section as a function of energy. The calculations are carried out by energy steps of 0.5 MeV. The RM and FEM methods yield results that are indistinguishable from those of the MN method, demonstrating their validity and accuracy for light systems.

We next consider the massive QE reaction  $^{48}\text{Ti} + ^{208}\text{Pb}$  [18], whose compound nucleus has  $Z = 104$ . The real and imaginary potential parameters, the vibrational states of the projectile and target are kept the same as those in Ref. [20]. The Coulomb barrier height is 195.40 MeV. In the following calculations, based on our tests, the  $R_{\max}$  is set to 50 fm to ensure sufficiently high accuracy for massive reactions, which have larger radii and stronger Coulomb interactions compared to lighter ones.

Fig. 1 shows the back-angle QE cross section relative to the Rutherford cross section as a function of  $L_{\max}$  at  $E_{c.m.} = 170.0$  MeV. The calculation is performed at  $170^\circ$  as the same as in Ref. [20]. The calculations consider vibrational couplings of the  $2^+$  state in the projectile  $^{48}\text{Ti}$  and up to five phonon excitations of the  $3^-$  state in the target  $^{208}\text{Pb}$ . The maximum angular momentum required for convergence reaches up to  $1000 \hbar$ . The RM and FEM methods demonstrate better stability and accuracy compared to the MN method, which starts to exhibit fluctuations beyond  $L_{\max} \approx 500 \hbar$ . One of the possible reasons for the fluctuation that happens when there are couplings might arise from that the wavefunctions differs by orders in different channels. The channels with low threshold energies easily destroy the linear independence of the solutions from  $r_{\min}$  to  $r_{\max}$  in the MN method as mentioned in Ref. [20]. In the following calculations, we have verified that the MN method has numerical instability problems for a large number of coupled channels, and the RM and FEM always produce indistinguishable results, which excellently confirm each other. Therefore, in the following figures, we plot only one line but use the label ‘‘RM / FEM’’ to indicate that the results are calculated by these two methods.

Fig. 2 presents the QE cross sections relative to the Rutherford cross section and the corresponding barrier distributions for  $^{48}\text{Ti} + ^{208}\text{Pb}$ . The barrier distribution is obtained by taking the derivative of the QE cross section with respect to energy. The experimental data are from Ref. [18]. Calculations with different coupling schemes are shown. The 1-1 coupling includes single-phonon excitations in both the projectile and the target, while the 1-3 coupling includes up to triple-phonon excitations in the target, as in Ref. [20]. Our results reproduce those of the previous work, showing multiple peaks in the barrier distribution. When we include up to five-phonon excitations in the target (1-5 coupling), some peaks in the barrier distribution disappear. And when 5-5 couplings are

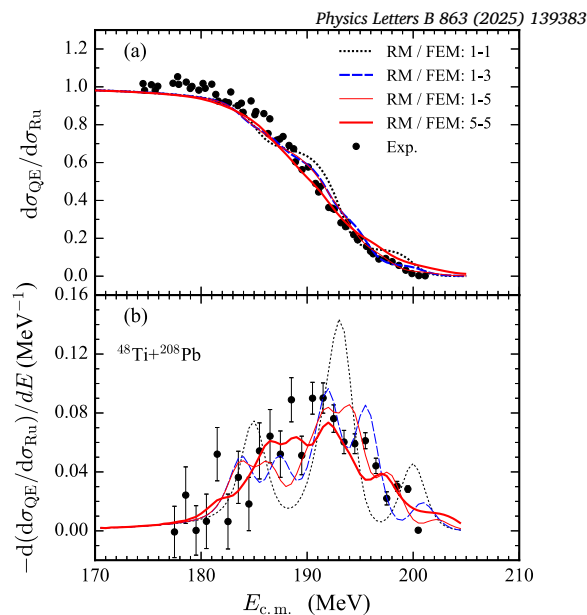


**Fig. 2.** (a) The back-angle QE cross section relative to the Rutherford cross section for  $^{48}\text{Ti} + ^{208}\text{Pb}$ . (b) The corresponding barrier distributions. The experimental data from Ref. [18] are shown as solid circles. The meanings of the symbols in the legend are the same as in Fig. 1, which are shown as dotted, dashed, thin and thick lines, respectively.

added in both the projectile and the target, we observe that the peaks in the barrier distribution become significantly smoothed, resulting in a single broad peak that better reproduces the general features of the experimental data. This indicates that multi-phonon states play a crucial role in smoothing the barrier distribution.

In the low energy region, current calculations underestimate the experimental data in Fig. 2. We have also examined the results of a nearby reaction,  $^{54}\text{Cr} + ^{208}\text{Pb}$ , measured by the same group, as shown in Fig. 2 in the supplementary material. The same potential parameters as in Ref. [20] are used. It is evident that at lower energies, the theoretical calculations describe the experimental data more reasonably, and multi-phonon couplings are important to smooth the barrier distribution. This suggests that the couplings associated with the unique structure of  $^{48}\text{Ti}$  may not have been fully included, leading to the underestimation of the experimental data in the low-energy region.

Our conclusions are similar to those of Ref. [29], where the five phonon couplings could play a significant role in the barrier distributions. However, as also mentioned in Ref. [29], we have currently poor empirical knowledge of the nuclear structure at such high excitation energies and many other reaction channels may also affect the barrier distribution. More endeavors are necessary for the investigations of a credible nuclear structure input to explain the measured barrier distribution in detail in the future.

We also study the QE reaction  $^{51}\text{V} + ^{248}\text{Cm}$ , whose compound nucleus has  $Z = 119$ . This reaction is relevant for the synthesis of super-heavy elements [24]. The real and imaginary potential parameters, the vibrational states of the projectile, and the transfer coupling parameters are taken from Table I of Ref. [24]. The Coulomb barrier height is 225.62 MeV. The calculation is performed at  $180^\circ$ . The target nucleus  $^{248}\text{Cm}$  has a well-developed rotational band due to its strong deformation [30]. In the legends, for example, 2-10 means the vibrational phonon number of the projectile  $N_{\text{vib}}^{\text{Proj}} = 2$  and the rotational levels of the target  $N_{\text{rot}}^{\text{Targ}} = 10$ , namely  $2^+, 4^+, \dots, 20^+$  are included together with the ground state, where convergence has been achieved. The extra symbol ‘‘-T’’ denotes the extra consideration of the transfer channels in the CC calculation.

Fig. 3 shows the QE cross sections and barrier distributions for different coupling schemes, compared with experimental data from Ref. [24].

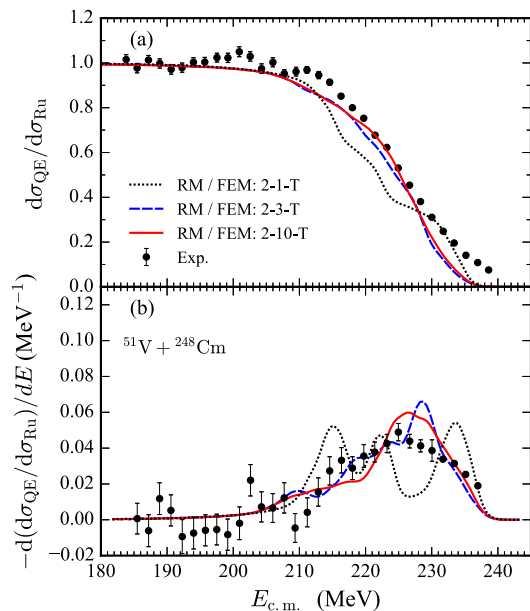


**Fig. 3.** Same as Fig. 2 but for  $^{51}\text{V} + ^{248}\text{Cm}$ . The experimental data from Ref. [24] are shown as solid circles. The number combinations in the legend denote the number of phonons used in vibrational couplings for the projectile  $N_{\text{vib}}^{\text{Proj}}$  and the number of excited states included in rotational couplings for the target  $N_{\text{rot}}^{\text{Targ}}$ . The extra symbol “-T” denotes the extra consideration of the transfer channels in the CC calculation. The Coulomb barrier height is 225.62 MeV.

Including more rotational states in the target (e.g., from 2-1-T to 2-3-T and 2-10-T) significantly enhances the QE cross section and smooths the barrier distribution, resulting in better agreement with the experimental data. This demonstrates the importance of including higher rotational excitations in the CC calculations for deformed heavy nuclei. The calculations still do not fully reproduce the experimental data, especially in the knee region, indicating that additional mechanisms may need to be included. Possible contributions from insufficient consideration of the potential parameters and transfer strength, single-particle excitations, multinucleon transfer, and quantum dissipation effects [15–17,46,47], as well as the multiple rotational bands [48] could play roles in further smoothing the barrier distributions for such heavy systems. Besides, for the sake of comparison, we use the previous potential parameters, which were adjusted depending on the experimental data. More systematic studies on the potentials for massive reactions are also needed.

For light reactions, capture is the same as fusion. While for massive reactions, capture refers to the scenario where the projectile and target make contact after Coulomb barrier to form a di-nuclear system, with their separation distance being smaller than the Coulomb radius. Fusion means that the di-nuclear system evolve to a compound nuclei after the capture [49]. Since the experimental and theoretical barrier distribution shapes of capture and QE reactions are similar [16], the CC approach that describes the QE data can also provide significant insights into capture cross sections, which are the primary step for fusion processes leading to superheavy element synthesis. Fig. 3 in the supplementary material shows the capture cross sections for  $^{51}\text{V} + ^{248}\text{Cm}$  under different coupling schemes. The inclusion of higher rotational excitations in the target (from 2-1-T to 2-10-T) significantly enhances the sub-barrier cross sections and decreases the above-barrier cross sections. It can also be observed from the Fig. 4 in the supplementary material that including more reaction channels generally increases the  $S$ -factor in the low-energy region. This suggests that high-spin state excitations couplings affect the capture probability at different energies. The MN method exhibits fluctuations in the sub-barrier region due to numerical instabilities, while the RM and FEM methods provide smooth and reliable results. The capture cross sections calculated here can be used

as input for other fusion or multinucleon transfer models to study the synthesis of superheavy nuclei [49–54].

Finally, we compare the results of OA formula and CC model in massive reactions involving the  $^{248}\text{Cm}$  target, using two projectiles,  $^{16}\text{O}$  and  $^{51}\text{V}$ , under various coupling conditions. The potential parameters are identical to those used in Ref. [24]. The excitation energy of the first rotational level for  $^{248}\text{Cm}$  is  $E_{\text{rot}} = 0.043$  MeV. For simplicity, only the quadrupole deformation parameter  $\beta_2 = 0.286$  for  $^{248}\text{Cm}$  is considered, and no vibrational couplings for the projectile are included. From Fig. 4(a-d), it can be observed that the results obtained using the OA formula are identical to the CC calculations with  $E_{\text{rot}} = 0$  MeV for both the  $^{16}\text{O} + ^{248}\text{Cm}$  and  $^{51}\text{V} + ^{248}\text{Cm}$  systems. However, the deviation between the OA formula and CC calculations with finite  $E_{\text{rot}}$  is significantly larger for the  $^{51}\text{V} + ^{248}\text{Cm}$  reaction compared to the  $^{16}\text{O} + ^{248}\text{Cm}$  reaction. This confirms the conclusion drawn in Ref. [55]: the OA approximation gradually loses its accuracy with increasing charge product of the projectile and target nuclei due to the effects of finite excitation energy of the target. However, when rotational couplings coexist with other couplings involving finite excitation energy, such as the transfer couplings, the coupling matrix becomes distance dependent and cannot be diagonalized or fully decoupled. Consequently, the results obtained using the OA formula differ significantly from CC results when the excitation energy is finite or zero in Fig. 4(e-f).

In summary, we have applied the sophisticated RM and FEM methods within the theoretical CC framework to describe massive QE reactions. By including the coupling with multi-phonon and high-spin states, we have investigated their roles in smoothing the barrier distributions and improving the agreement with experimental data for the reactions  $^{48}\text{Ti} + ^{208}\text{Pb}$  and  $^{51}\text{V} + ^{248}\text{Cm}$ . Our results demonstrate that the RM and FEM methods are much more stable and accurate than the MN method for massive reactions containing many coupled channels and requiring high angular momenta. The collective excitations significantly influence the QE barrier distributions, indicating the necessity of including them for accurate descriptions. The applicability of the OA formula is further investigated, revealing evident deviations from the CC results when the formula is applied in massive reactions and the presence of additional coupling channels beyond collective rotation, such as in cases involving transfer coupling. Although our calculations have not fully reproduced the experimental data, they highlight the importance of multi-phonon and high-spin states and suggest that other reaction mechanisms, such as single-particle excitations, multinucleon transfer, and dissipative effects, may need to be considered. Future work should focus on systematically including these effects and obtaining correct nuclear structure inputs for the multiphonon couplings. Furthermore, the numerical methods proposed in this work could advance the research on the synthesis of superheavy nuclei by providing improved barrier information and capture cross sections. They could also offer valuable insights into astrophysically important deep sub-barrier fusion reactions, such as  $^{12}\text{C} + ^{12}\text{C}$  at very low energies, by providing high-accuracy solutions of the coupled-channel equations.

#### Declaration of competing interest

The authors declare that they have no known competing financial interests or personal relationships that could have appeared to influence the work reported in this paper.

#### Acknowledgement

We thank Profs. K. Hagino and E. Piasecki for help during this work. This work is supported by the National Key R&D Program of China (Contract Nos. 2024YFE0109804, 2022YFA1602302, 2023YFA1606402), the National Natural Science Foundation of China (Grants Nos. 12375130, 12235020), the Continuous Basic Scientific Research Project, Basic Research Special Zone, the Director’s Foundation of Department of Nuclear Physics (12SZJJ-202305), the Dean’s Foundation of China

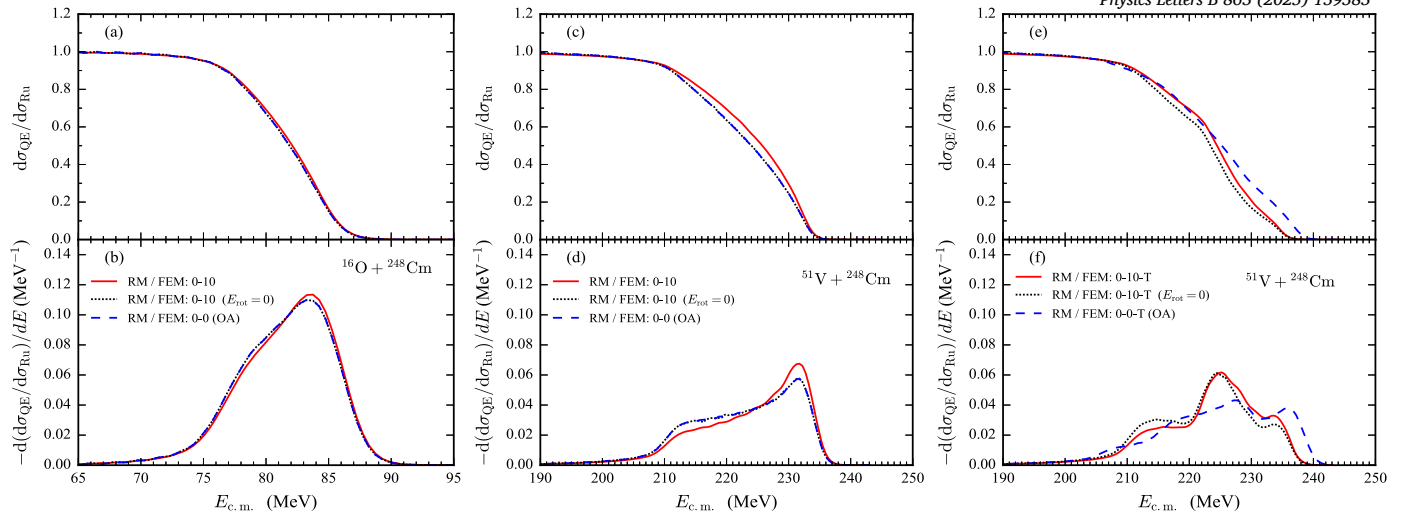


**Fig. 4.** Same as Fig. 3 but for  $^{16}\text{O}$ ,  $^{51}\text{V} + ^{248}\text{Cm}$  under the indicated couplings. The calculations with finite  $E_{\text{rot}}$ ,  $E_{\text{rot}} = 0$  MeV and OA formula are denoted as solid, dotted and dashed lines. .

Institute of Atomic Energy (12YZ010270624219), and the Peoples' Friendship University of Russia (RUDN) Strategic Academic Leadership Program (project No. 021934-0-00).

## Appendix A. Supplementary material

Supplementary material related to this article can be found online at <https://doi.org/10.1016/j.physletb.2025.139383>.

## Data availability

Data will be made available on request.

## References

- [1] K. Hagino, K. Ogata, A.M. Moro, *Prog. Part. Nucl. Phys.* 125 (2022) 103951.
- [2] K. Hagino, N. Rowley, *Phys. Rev. C* 69 (2004) 054610.
- [3] P.W. Wen, C.J. Lin, H.M. Jia, L. Yang, F. Yang, D.H. Huang, T.P. Luo, C. Chang, M.H. Zhang, N.R. Ma, *Phys. Rev. C* 105 (2022) 034606.
- [4] L. Yang, C.J. Lin, H.M. Jia, D.X. Wang, N.R. Ma, L.J. Sun, F. Yang, X.X. Xu, Z.D. Wu, H.Q. Zhang, Z.H. Liu, *Phys. Rev. Lett.* 119 (2017) 042503.
- [5] L. Yang, C.J. Lin, H. Yamaguchi, A.M. Moro, N.R. Ma, D.X. Wang, K.J. Cook, M. Mazzocco, P.W. Wen, S. Hayakawa, et al., *Nat. Commun.* 13 (2022) 7193.
- [6] C.J. Lin, *Heavy-Ion Nuclear Reactions*, Harbin, Engineering University Press, Harbin, 2015.
- [7] M. Dasgupta, D.J. Hinde, N. Rowley, A.M. Stefanini, *Annu. Rev. Nucl. Part. Sci.* 48 (1998) 401.
- [8] J.R. Leigh, M. Dasgupta, D.J. Hinde, J.C. Mein, C.R. Morton, R.C. Lemmon, J.P. Lestone, J.O. Newton, H. Timmers, J.X. Wei, N. Rowley, *Phys. Rev. C* 52 (1995) 3151.
- [9] H.M. Jia, C.J. Lin, F. Yang, X.X. Xu, H.Q. Zhang, Z.H. Liu, Z.D. Wu, L. Yang, N.R. Ma, P.F. Bao, L.J. Sun, *Phys. Rev. C* 90 (2014) 031601(R).
- [10] Y.K. Gupta, B.K. Nayak, U. Garg, K. Hagino, K.B. Howard, N. Sensharma, et al., *Phys. Lett. B* 806 (2020) 135473.
- [11] Y.K. Gupta, V.B. Kataria, G.K. Prajapati, K. Hagino, D. Patel, V. Ranga, U. Garg, L.S. Danu, A. Pal, et al., *Phys. Lett. B* 845 (2023) 138120.
- [12] E. Piasecki, Ł. Świdorski, W. Gawlikowicz, J. Jastrzębski, N. Keeley, M. Kisieliński, et al., *Phys. Rev. C* 80 (2009) 054613.
- [13] S. Yusa, K. Hagino, N. Rowley, *Phys. Rev. C* 85 (2012) 054601.
- [14] G. Pollaro, *Phys. Rev. Lett.* 100 (2008) 252701.
- [15] E. Piasecki, M. Kowalczyk, S. Yusa, A. Trzcińska, K. Hagino, *Phys. Rev. C* 100 (2019) 014616.
- [16] G. Colucci, E. Piasecki, A. Trzcińska, P.W. Wen, V. Palmin, T. Abramova, et al., *Phys. Rev. C* 109 (2024) 014610.
- [17] K.J. Cook, D.C. Rafferty, D.J. Hinde, E.C. Simpson, M. Dasgupta, L. Corradi, et al., *Nat. Commun.* 14 (2023) 3061.
- [18] S. Mitsuoka, H. Ikezoe, K. Nishio, K. Tsuruta, S.C. Jeong, Y. Watanabe, *Phys. Rev. Lett.* 99 (2007) 182701.
- [19] S.S. Ntshangase, N. Rowley, R.A. Bark, S.V. Försch, J.J. Lawrie, E.A. Lawrie, et al., *Phys. Lett. B* 651 (2007) 27.
- [20] M.Z. Farhan, K. Hagino, S. Mitsuoka, H. Ikezoe, *Phys. Rev. C* 77 (2008) 034604.
- [21] Y.T. Oganessian, V.K. Utyonkov, Y.V. Lobanov, F.S. Abdullin, A.N. Polyakov, et al., *Phys. Rev. C* 74 (2006) 044602.
- [22] T. Tanaka, Y. Narikiyo, K. Morita, K. Fujita, D. Kaji, K. Morimoto, S. Yamaki, Y. Wakabayashi, et al., *J. Phys. Soc. Jpn.* 87 (2018) 014201.
- [23] T. Tanaka, K. Morita, K. Morimoto, D. Kaji, H. Haba, R.A. Boll, N.T. Brewer, S. Van Cleve, D.J. Dean, et al., *Phys. Rev. Lett.* 124 (2020) 052502.
- [24] M. Tanaka, P. Brionnet, M. Du, J. Ezold, K. Felker, B.J.P. Gall, S. Go, R.K. Grzywacz, H. Haba, K. Hagino, et al., *J. Phys. Soc. Jpn.* 91 (2022) 084201.
- [25] K. Hagino, N. Rowley, A.T. Kruppa, *Comput. Phys. Commun.* 123 (1999) 143.
- [26] <https://www2.yukawa.kyoto-u.ac.jp/~kouichi.hagino/ccfull.html>.
- [27] G. Kaur, T. Banerjee, N. Kumar, K. Kapoor, A. Jhingan, N. Rowley, M. Thakur, A. Yadav, R. Mahajan, N. Saneesh, *Acta Phys. Pol. B* 49 (2018) 651.
- [28] H. Esbensen, *Phys. Rev. C* 72 (2005) 054607.
- [29] H. Esbensen, C.L. Jiang, *Phys. Rev. C* 79 (2009) 064619.
- [30] <https://www.nndc.bnl.gov/nudat3/>.
- [31] P.W. Wen, O. Chuluunbaatar, A.A. Gusev, R.G. Nazmitdinov, A.K. Nasirov, S.I. Vinitzky, C.J. Lin, H.M. Jia, *Phys. Rev. C* 101 (2020) 014618.
- [32] P.W. Wen, C.J. Lin, R.G. Nazmitdinov, S.I. Vinitzky, O. Chuluunbaatar, A.A. Gusev, A.K. Nasirov, H.M. Jia, A. Gózdź, *Phys. Rev. C* 103 (2021) 054601.
- [33] P. Descouvemont, D. Baye, *Rep. Prog. Phys.* 73 (2010) 036301.
- [34] P. Descouvemont, M.S. Hussein, *Phys. Rev. Lett.* 111 (2013) 082701.
- [35] P. Descouvemont, *Comput. Phys. Commun.* 200 (2016) 199.
- [36] Shubhchintak, P. Descouvemont, *Phys. Lett. B* 811 (2020) 135874.
- [37] O. Chuluunbaatar, A.A. Gusev, A.G. Abrashkevich, A. Amaya-Tapia, M.S. Kaschiev, S.Y. Larsen, S.I. Vinitzky, *Comput. Phys. Commun.* 177 (2007) 649.
- [38] O. Chuluunbaatar, A.A. Gusev, S.I. Vinitzky, A.G. Abrashkevich, *Comput. Phys. Commun.* 179 (2008) 685.
- [39] A.A. Gusev, O. Chuluunbaatar, S.I. Vinitzky, A.G. Abrashkevich, *Comput. Phys. Commun.* 185 (2014) 3341.
- [40] T.P. Luo, P.W. Wen, C.J. Lin, L. Yang, H.M. Jia, F. Yang, D. Huang, C. Chang, M.H. Zhang, Y. Yang, T.H. Mo, N.R. Ma, *Chin. Phys. C* 46 (2022) 064105.
- [41] S.I. Vinitzky, P.W. Wen, A.A. Gusev, O. Chuluunbaatar, R.G. Nazmitdinov, A.K. Nasirov, C.J. Lin, H.M. Jia, A. Gózdź, *Acta Phys. Pol. B, Proc. Suppl.* 13 (2020) 549.
- [42] O. Chuluunbaatar, A.A. Gusev, S.I. Vinitzky, A.G. Abrashkevich, P.W. Wen, C.J. Lin, *Comput. Phys. Commun.* 278 (2022) 108397.
- [43] A.A. Gusev, O. Chuluunbaatar, V.L. Derbov, R.G. Nazmitdinov, S.I. Vinitzky, P.W. Wen, C.J. Lin, H.M. Jia, L.L. Hai, *Lect. Notes Comput. Sci.* 14139 (2023) 128.
- [44] M. Rhoades-Brown, M.H. Macfarlane, S.C. Pieper, *Phys. Rev. C* 21 (1980) 2417.
- [45] M. Rhoades-Brown, M.H. Macfarlane, S.C. Pieper, *Phys. Rev. C* 21 (1980) 2436.
- [46] A. Diaz-Torres, *Phys. Rev. C* 81 (2010) 041603(R).
- [47] I. Lee, A. Diaz-Torres, *Phys. Lett. B* 827 (2022) 136970.
- [48] D. Martyanov, E. Soukhovitskii, R. Capote, J.M. Quesada, S. Chiba, N. Shu, Y. Chen, W. Wang, H. Zhang, *EPJ Web Conf.* 239 (2020) 03003.
- [49] A.K. Nasirov, B.M. Kayumov, *Phys. Rev. C* 109 (2024) 024613.
- [50] P.W. Wen, C. Li, L. Zhu, C.J. Lin, F.S. Zhang, *J. Phys. G, Nucl. Part. Phys.* 44 (2017) 115101.
- [51] N. Tang, X.R. Zhang, J.J. Li, P.W. Wen, F.S. Zhang, *Phys. Rev. C* 106 (2022) 034601.
- [52] N. Wang, E.G. Zhao, W. Scheid, S.G. Zhou, *Phys. Rev. C* 85 (2012) 041601(R).
- [53] L. Zhu, J. Su, C. Li, F.S. Zhang, *Phys. Lett. B* 829 (2022) 137113.
- [54] M.H. Zhang, Y.H. Zhang, Y. Zou, C. Wang, L. Zhu, F.S. Zhang, *Phys. Rev. C* 109 (2024) 014613.
- [55] T. Rumin, K. Hagino, N. Takigawa, *Phys. Rev. C* 63 (2001) 044603.